

Article

CFD Analysis of Turbulent Flow of Power-Law Fluid in a Partially Blocked Eccentric Annulus

Ravi Singh ¹, Ramadan Ahmed ^{1,*}, Hamidreza Karami ¹, Mustafa Nasser ² and Ibelwaleed Hussein ²

¹ Mewbourne School of Petroleum and Geological Engineering, University of Oklahoma, Norman, OK 73019, USA; rasingh@ou.edu (R.S.); karami@ou.edu (H.K.)

² Gas Processing Center, College of Engineering, Qatar University, P.O. Box 2713, Doha, Qatar; m.nasser@qu.edu.qa (M.N.); ihussein@qu.edu.qa (I.H.)

* Correspondence: r.ahmed@ou.edu

Abstract: This study focuses on analyzing the turbulent flow of drilling fluid in inclined wells using the Computational Fluid Dynamics (CFD) technique. The analysis is performed considering an annulus with a fixed eccentricity of 90% and varying fluid properties, diameter ratio, and bed thickness to examine velocity profile, pressure loss, and overall wall and average bed shear stresses. CFD simulation results are compared with existing data for validation. The pressure loss predicted with CFD agrees with the data. After verification, predictions are used to establish a correlation that can be applied to compute bed shear stress. The established correlation mostly displays a discrepancy of up to 10% when compared with simulation data. The correlation can be used to optimize hole cleaning and manage downhole pressure.

Keywords: CFD; annular flow; bed shear stress; velocity profile; turbulent flow



Citation: Singh, R.; Ahmed, R.; Karami, H.; Nasser, M.; Hussein, I. CFD Analysis of Turbulent Flow of Power-Law Fluid in a Partially Blocked Eccentric Annulus. *Energies* **2021**, *14*, 731. <https://doi.org/10.3390/en14030731>

Academic Editor: Ergun Kuru
Received: 11 January 2021
Accepted: 25 January 2021
Published: 30 January 2021

Publisher's Note: MDPI stays neutral with regard to jurisdictional claims in published maps and institutional affiliations.



Copyright: © 2021 by the authors. Licensee MDPI, Basel, Switzerland. This article is an open access article distributed under the terms and conditions of the Creative Commons Attribution (CC BY) license (<https://creativecommons.org/licenses/by/4.0/>).

1. Introduction

Hydrocarbon production from horizontal and inclined wells is now a widespread practice. One of the major drawbacks of drilling horizontal and inclined wells is that the inclination causes wellbore eccentricity. This eccentric wellbore geometry causes a non-uniform fluid velocity profile in the annulus creating low-velocity stagnant regions to develop. The formation of the stagnant zones makes the cuttings removal process inefficient, leading to the development of stable solids beds. The formation of the bed restricts fluid flow and increases the pressure loss and bottom hole pressure, which needs to be maintained within the operating pressure window to prevent drilling problems.

Failure in ensuring a good hole cleaning leads to several drilling issues such as formation damage, fluid loss, lost circulation, high torque and drag, or stuck pipe. Therefore, a wellbore hydraulic study is vital in establishing a precise model to compute the pressure loss in the annulus and optimize hole cleaning. Several studies [1–7] have been performed to examine the flow in an annular region and develop effective hole cleaning solutions and manage wellbore pressure within the operating window. For an effective hole cleanup, the enhancement of bed shear stress and local fluid velocity on the bed surface is vital. If the flow rate is increased, the solids bed thickness would decrease. However, an increase in pressure due to the flow rate increase can offset the decline in frictional resistance achieved because of bed thickness reduction. Therefore, an accurate bed shear stress model is required for hydraulic optimization. The model should account for the bed shear stress variation occurring because of bed thickness variation.

Common flow parameters in the wellbore such as bed shear stress and pressure loss are affected by mudflow rate, fluid properties, and wellbore geometry (eccentricity, bed height, and diameter ratio). The development of solids beds makes the wellbore flow geometry complicated; consequently, analytical solutions are not possible to establish when a stationary solids bed is formed. A CFD investigation is frequently preferred approach

to study the connection among relevant flow parameters (pressure loss, bed shear stress, and flow rate) in eccentric annuli. Previously, CFD models [7–12] for partially blocked annuli were established considering laminar flow conditions. Similar studies [13–17] were performed to analyze laminar flows in concentric and eccentric annuli.

Based on the CFD analysis of eccentric annular flow, Rojas et al. [7] showed the impact of the level of annular blockage on the bed shear stress under laminar flow conditions. The bed shear stress exhibited significant reduction with a decrease in the bed thickness. Results also demonstrated substantial variation in the bed shear stress in the lateral direction, which causes non-uniform bed erosion. Similar results were obtained for a concentric annulus [8]. The results indicated the reduction of local fluid velocity and bed shear stress with an increase in the blockage level. These studies demonstrated that the impact of blockage on relevant flow parameters such as pressure loss and bed shear stress can be predicted with reasonable accuracy with the application of CFD techniques.

The flow behavior of most drilling fluids used in the industry is best described using the power-law rheology model. The flow regime in inclined wells can be laminar or turbulent depending on fluid viscosity, borehole geometry, and fluid velocity. Even the effects of bed formation on the hydraulics of annular flows have been studied recently [7–12], the impact of bed thickness on the hydraulic parameters (pressure loss and bed shear stress) of turbulent flow in a partially blocked eccentric annulus has not been previously investigated. The goal of this investigation is to study the turbulent flow of power-law fluid in wellbores considering eccentric annuli with blockage and develop a relationship between bed shear stress and the level of blockage.

2. Theoretical Background

For non-Newtonian fluid, the Reynolds number in a concentric annulus is defined as a function of apparent viscosity, which is determined by equating the non-Newtonian pressure loss equation with that of a Newtonian fluid. Thus:

$$Re^* = \frac{\rho \bar{V} D_e}{\mu_a} \quad (1)$$

where D_e is the effective diameter, which is determined from the hydraulic diameter of the annulus as: $D_e = 0.81 D_h$. K is fluid consistency index, \bar{V} is average fluid velocity and μ_a is the apparent viscosity of the fluid. The hydraulic diameter for any non-circular duct is generally expressed as: $D_h = 4A/P_w$, where P_w is the wetted perimeter of the annulus, and A represents the cross-sectional area of the flow. The apparent viscosity of power-law fluid ($\tau = K\dot{\gamma}^n$) in a concentric annulus is computed as:

$$\mu_a = K \left(\frac{2n+1}{3n} \right)^n \left(\frac{12\bar{V}}{D_h} \right)^{n-1} \quad (2)$$

Equation (2) is adopted for partially blocked annulus using the hydraulic diameter concept. The Fanning friction factor (f) is determined from the mean fluid velocity (\bar{V}) and the overall wall shear stress ($\bar{\tau}_w$) as:

$$f = \frac{\bar{\tau}_w}{\rho \bar{V}^2 / 2} \quad (3)$$

where ρ is the fluid density. Applying the momentum balance, the average/overall wall shear stress is calculated from the pressure gradient as:

$$\bar{\tau}_w = \frac{D_h}{4} \frac{dP}{dL} \quad (4)$$

According to Kozicki et al. [18], dimensionless geometric parameters can be utilized to determine the Reynolds number to estimate the pressure loss in a non-circular duct of any

arbitrary cross-section. For a partially blocked eccentric annulus, Rojas et al. [7] presented correlations for determining the geometric parameters. Kozicki et al. [18] proposed a generalized Reynolds number for non-circular duct flows. Thus:

$$Re_g = \frac{\rho \bar{V}^{2-n} D_h^n}{8^{n-1} K \left(\frac{a+bn}{n} \right)^n} \quad (5)$$

where a and b are the dimensionless parameters and n is the fluid behavior index.

In inclined wellbores, the development of solids beds influences the wall shear stress and velocity profiles [9]. Thus, the bed shear stress (i.e., the average shear stress acting on the bed) could significantly vary from the overall wall shear stress. The bed shear stress ($\bar{\tau}_{bed}$) governs the movement of bed particles by affecting the hydrodynamic forces (lift and drag) acting on the bed particles. By determining the pressure loss, the overall wall shear stress ($\bar{\tau}_w$) can be predicted and hydraulic optimization can be performed to ensure efficient hole cleaning in highly deviated wells [7,8,19,20]. Previous studies [10,12] were conducted to investigate the impact of blockage on annular flows. The bed shear stress [7,21] is a relevant flow parameter for accurate hydraulic modeling of the wellbore. The dimensionless bed shear stress (π_{bed}) is defined as [7]:

$$\pi_{bed} = \left(\frac{\bar{\tau}_{bed}}{\bar{\tau}_w} \right)^n \quad (6)$$

The bed shear stress is defined in this form to reduce the number of flow parameters that affect its magnitude.

3. Modeling Flow in Partially Block Eccentric Annulus

The research methodology utilized to achieve the principal objective of this study includes CFD analysis of a partially blocked eccentric annular flow using commercial software (ANSYS Fluent) to establish a relationship between the bed shear stress and the blockage thickness. To conduct the analysis, several 3D models of annular geometries (varying geometric dimensions and blockage level) are created to simulate and examine the bed shear stress and frictional pressure loss. The simulation is performed considering turbulent flow conditions and varying flow behavior of the fluid and the annular geometry. Using results obtained from CFD simulations, a simplified correlation is developed to calculate the bed shear stress in eccentric annuli as a function of bed height. The correlation is valid for power-law fluids flowing in highly eccentric annuli (approximately 90%) when the bed thickness is between zero and 100 percent of the inner pipe diameter.

To develop a theoretical model, the following assumptions are made: (i) the flow is considered as a fully developed turbulent flow under steady-state condition; (ii) the fluid is considered incompressible and flowing under isothermal conditions, (iii) the flow behavior of the fluid is described using the power-law fluid rheology model; (iv) non-rotating inner pipe; (v) no-slip condition at the surface of the bed and other wetted surfaces; (vi) stable and uniform solids bed; (vii) no impact of suspended solids on the flow; and (viii) all wetted surfaces are smooth.

3.1. Governing Equation

A variety of turbulent modeling approaches have been established to determine the approximate solutions for the equations of motion. One of these models is the k - ϵ model that is often applied to model turbulent flows in uniform ducts such as eccentric annulus [22] and open channels. In the standard k - ϵ model, the turbulent kinetic energy (k) distribution is described as:

$$\frac{\partial(\rho k)}{\partial t} + \frac{\partial(\rho k u_i)}{\partial x_i} = \frac{\partial}{\partial x_j} \left[\left(\mu + \frac{\mu_t}{\sigma_k} \right) \frac{\partial k}{\partial x_j} \right] + G_k + G_b - \rho \epsilon - Y_M + S_k \quad (7)$$

Similarly, the turbulent energy dissipation rate (ϵ) is described using the following differential equation.

$$\frac{\partial(\rho\epsilon)}{\partial t} + \frac{\partial(\rho\epsilon u_i)}{\partial x_i} = \frac{\partial}{\partial x_j} \left[\left(\mu + \frac{\mu_t}{\sigma_\epsilon} \right) \frac{\partial \epsilon}{\partial x_j} \right] + C_{1\epsilon} \frac{\epsilon}{k} (G_k + C_{3\epsilon} G_b) - C_{2\epsilon} \rho \frac{\epsilon^2}{k} + S_\epsilon \quad (8)$$

where G_k is the turbulent kinetic energy generated because of the mean velocity gradient. Y_M is fluctuating dilatation in incompressible turbulence to the overall dissipation rate. G_b is the turbulent kinetic energy developed due to the buoyancy. σ_k and σ_ϵ are the turbulent Prandtl numbers for k and ϵ , respectively. $C_{1\epsilon}$, $C_{2\epsilon}$, $C_{3\epsilon}$ and C_μ are the k - ϵ model constants. The values of the turbulent Prandtl numbers and model constants are [23,24]: $C_{1\epsilon} = 1.44$, $C_{2\epsilon} = 1.92$, $C_\mu = 0.09$, $\sigma_k = 1.0$, $\sigma_\epsilon = 1.3$. In the standard k - ϵ model, the Reynolds stresses are obtained using the eddy viscosity (μ_t) that is given by:

$$\mu_t = \rho C_\mu \frac{k^2}{\epsilon} \quad (9)$$

For power-law fluid, the viscous shear stress is computed from the shear rate ($\dot{\gamma}$) as: $\tau = K\dot{\gamma}^n$. The apparent viscosity ($\mu(\dot{\gamma}) = \tau/\dot{\gamma}$) of non-Newtonian fluids is expressed in terms of the shear rate, which is defined in a general form as:

$$|\dot{\gamma}|^2 = 2 \left[\left(\frac{\partial u}{\partial x} \right)^2 + \left(\frac{\partial v}{\partial y} \right)^2 + \left(\frac{\partial w}{\partial z} \right)^2 \right] + \left(\frac{\partial u}{\partial y} + \frac{\partial v}{\partial x} \right)^2 + \left(\frac{\partial v}{\partial z} + \frac{\partial w}{\partial x} \right)^2 + \left(\frac{\partial v}{\partial z} + \frac{\partial w}{\partial y} \right)^2 \quad (10)$$

This relationship helps evaluate the stress terms in the equation of motion. u , v , and w are time-averaged local fluid velocities in the x , y , and z directions. Using these velocities, the Reynolds Averaged Navier–Stokes (RANS) equation for incompressible fluid can be described in a generalized form as:

$$\rho \left(\frac{\partial u_i}{\partial t} + u_j \frac{\partial u_i}{\partial x_j} \right) = - \frac{\partial p}{\partial x_i} + \frac{\partial}{\partial x_j} (\mu \dot{\gamma} + \mu_t \dot{\gamma}) + F_i \quad (11)$$

where F_i is the body force. u_i is the time-averaged local fluid velocity in the direction x_i . The continuity equation for incompressible fluid is described as:

$$\frac{\partial u_j}{\partial x_j} = 0 \quad (12)$$

The model equations (Equations (7)–(12)) are solved numerically in the CFD software using the finite volume method implemented on a computational grid system with reasonable grid size.

3.2. Geometry Creation and Mesh Generation

A precise representation of the flow geometry is essential in performing extensive CFD simulations. The first step in a CFD modeling process is the flow geometry creation, which is followed by mesh generation (Figure 1). Numerous flow geometries are created varying bed height (0 to 100%) and diameter ratio ($\kappa = D_i/D_o$). To cover a wide range of wellbore geometries, three diameter ratios (25, 50, and 75%) are considered. The relative eccentricity ($e = d/(R_0 - R_i)$) considered for all the simulation cases is 90%, where R_i and R_0 are the diameters of the inner and outer pipes, respectively; and d is the offset distance between the centers of the pipes.

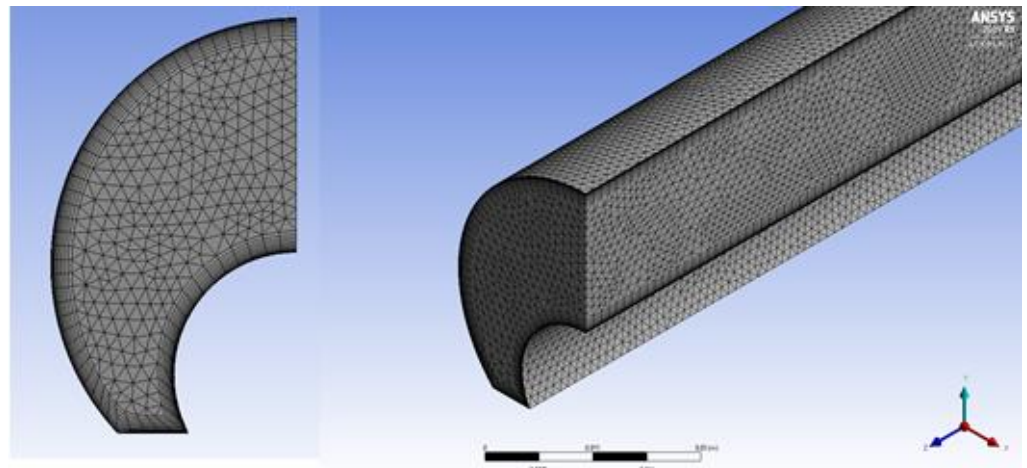


Figure 1. Unstructured grid system in a partially blocked annulus [25].

The second step after the creation of the flow geometry is the appropriate mesh generation. The grids (mesh) are generated to represent the entire flow domain and ensure the required numerical precision, which is determined by the number of grid points. The numerical accuracy and grid resolution increase with the number of grids. However, the number of grids needs to be optimized to avoid very long computational time. The unstructured grid system (Figure 1) is utilized in this study to ensure accuracy with a reasonable computational time.

3.3. Boundary Conditions

Implementing the correct boundary conditions is paramount before beginning a numerical simulation. Boundary conditions are essential to represent real scenarios of flow conditions at the flow boundaries. Five named surfaces (Figure 2) are considered as flow boundaries, which are grouped into three subcategories as follows:

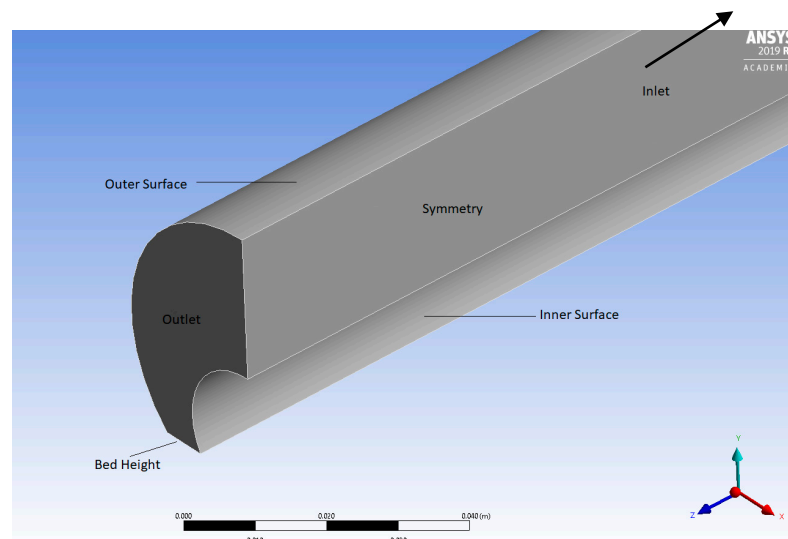


Figure 2. Named faces of the flow geometry [25].

Inlet (Fluid Inflow): The inlet face is named as inlet boundary (velocity inlet) located at the upstream end of the simulated wellbore at which the velocity profile is assumed uniform.

Outlet (Fluid Outflow): A pressure outlet boundary condition is defined at the 3D geometries outflow, which is located downstream of the simulated wellbore.

Wall Boundaries: The no-slip boundary condition is implemented in all walled surfaces, namely Bed Surface, Inner Surface, and Outer Surface in the CFD solver. The volume enclosed by these three wall boundaries (named surfaces) forms the flow domain (simulated wellbore).

3.4. Numerical Setup in Fluent Solver

The CFD final result needs to be independent of the initial conditions. Thus, a steady-state pressure-based technique is chosen to model turbulent flow in annuli with stationary cuttings bed. The technique is one of the most reliable and commonly used methods to model and analyze turbulent fluid flow. Apart from this, the pressure gradient effect and enhanced wall treatment options are selected to maintain the required numerical accuracy at the flow boundaries. Furthermore, the Semi-Implicit Pressure Linked Equation (SIMPLE) algorithm is implemented in combination with the second-order discretization method for momentum, turbulent dissipation rate, turbulent kinetic energy, and pressure. The convergence limit for the continuity equation is maintained at 1×10^{-4} and the convergence requirements for momentum, kinetic energy, dissipation rate equations are set at 1×10^{-7} [26].

3.5. Grid Sensitivity Analysis

Mesh size sensitivity analysis is performed to ensure the accuracy of CFD simulations. Input parameters for the grid-independent study are presented in Table 1. The input parameters are the specified boundary conditions. The grid system considered for this analysis is based on different grid refinement levels (0.5, 1.25, 2.5, and 5 million grids/elements). All simulations are conducted maintaining a high Reynolds number ($Re^* > 14,000$). Figure 3 demonstrates an increase in accuracy with the number of grids that improves numerical accuracy. After maintaining a mesh of size of more than 2.2 million grids, the pressure gradient stabilizes [25].

Table 1. Inputs used for simulation.

Parameters	Value
Drill Pipe Diameter, D_i (m)	0.025
Casing Diameter, D_o (m)	0.05
Diameter Ratio, κ	0.5
Relative Eccentricity, e	0.9
Solid Bed Height, H_{bed} (%)	30
Fluid Flow Rate, Q (m^3/s)	5×10^{-5}
Fluid Density, ρ (kg/m^3)	1000
Consistency Index, K (Pas^n)	5×10^{-5}
Fluid Behavior Index, n	1

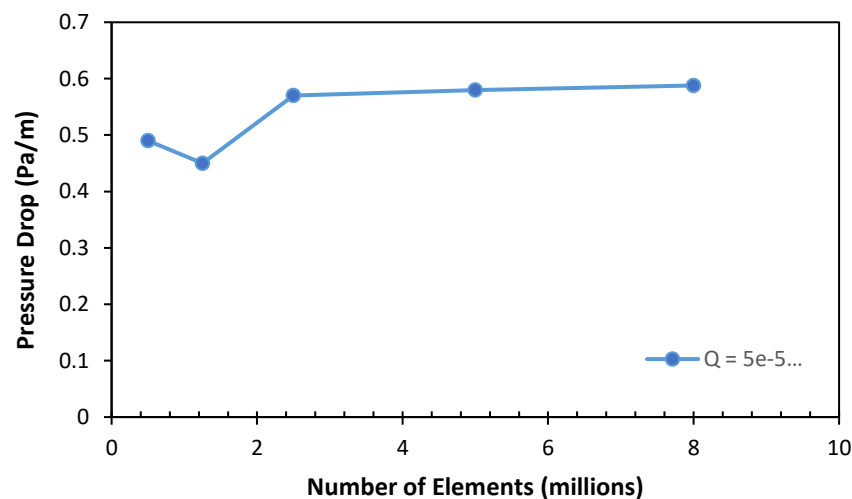


Figure 3. Grid independent study for various numbers of grids [25].

4. Validation of CFD Simulation Results

To validate the accuracy of the simulation approach implemented, the CFD results are compared with available pressure gradient measurements obtained from eccentric annulus (8 in × 4.5 in) with a recorded average bed thickness [27,28]. The measurements are obtained for diverse bed heights, fluid properties (Table 2), and flow rates. Four water-based muds are considered. During the experiment, the flow rate was between 150 and 400 gal/min. The Reynolds numbers (Re^*) of the flows are determined to distinguish the flow regime. Figure 4 compares experimental measurements with CFD simulation results. The results are predominately in agreement with measurements. Under laminar flow conditions (Figure 4c), the discrepancies are considerable (around 30%). The predictions are reasonably accurate with a maximum discrepancy of about 17% under turbulent flow conditions. The Reynolds number (Re^*) obtained from Equation (1) is valid for a concentric annulus. Hence, it is an approximate indicator of the flow regime when used in partially blocked eccentric annuli. Hence, some of the low Reynolds number flow data points may not represent turbulent flows even though they are more than 2100.

Table 2. Properties of fluids used for CFD validation.

Fluid Type	Fluid Behavior Index (n)	Consistency Index K (Pas ^{n})
Mud A	0.65	0.061
Mud B	0.52	0.408
Mud C	0.56	0.566
Mud D	0.69	0.140

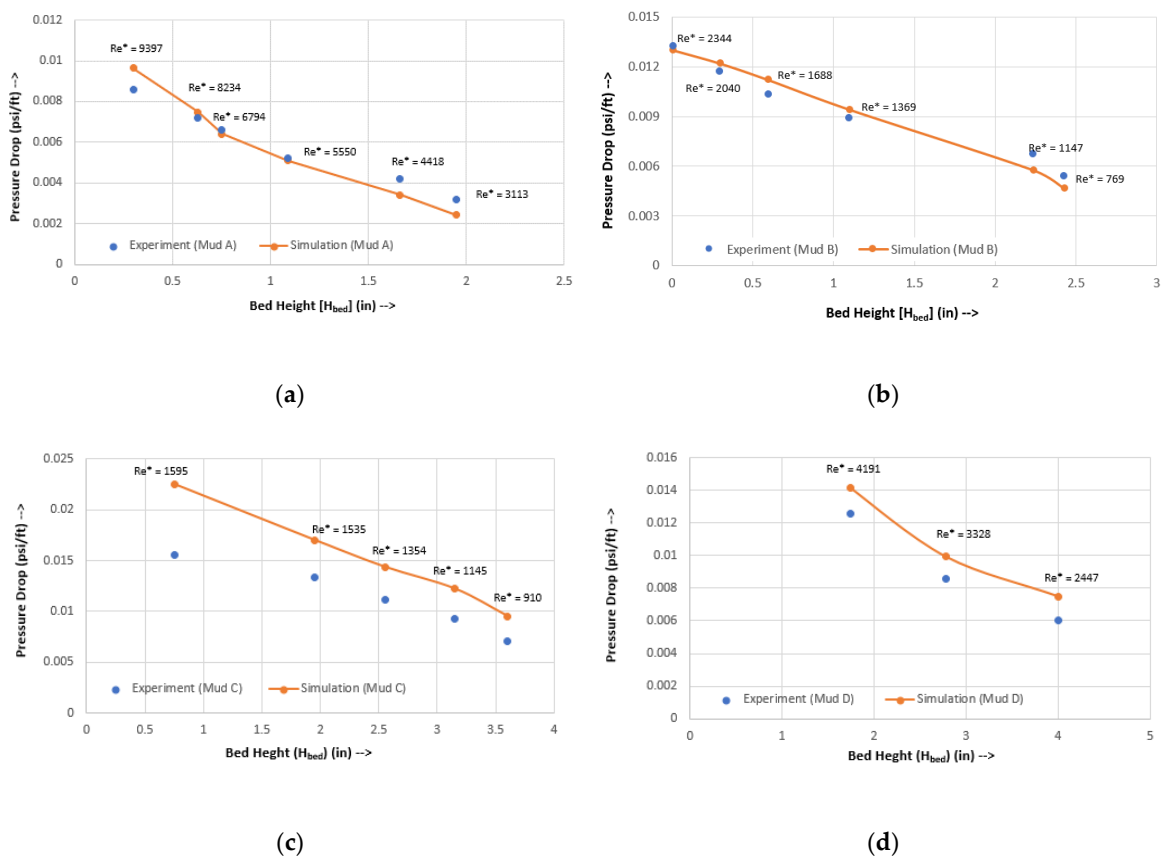


Figure 4. Comparison of CFD prediction with experimental measurement: (a) Mud A; (b) Mud B; (c) Mud C; and (d) Mud D.

5. Parametric Study

A parametric study is conducted to examine how the annular pressure loss is affected by the diameter ratio and bed height. Simulations are conducted maintaining high Reynolds numbers and varying the relevant flow parameters including diameter ratio, bed height, and flow behavior index. All the CFD simulation cases considered in this study were performed at a constant flow rate of $5 \times 10^{-5} \text{ m}^3/\text{s}$. The fluid density and hole diameter are fixed at $1000 \text{ kg}/\text{m}^3$ and 0.05 m , respectively.

5.1. Annular Frictional Pressure Loss

CFD simulations are performed to calculate the annular pressure loss for dimensionless bed height ($H_{bed} = h/D_i$) ranging from 0 to 100 percent. h is the bed height measured from the bottom of the outer pipe/cylinder. A constant flow rate is maintained for all cases and the change in annular pressure gradient (dp/dz) is observed (Figure 5). With increasing bed height and diameter ratio the pressure loss sharply increased. This phenomenon is primarily attributed to the reduction in flow area caused by the increase in bed height and diameter ratio. The reduction in flow area considerably increases the average velocity, and subsequently, augments the pressure loss. Furthermore, the hydraulic resistance experienced by the fluid flowing through the annulus diminishes with a decrease in fluid behavior index due to the improvement in the shear-thinning tendency of the fluid.

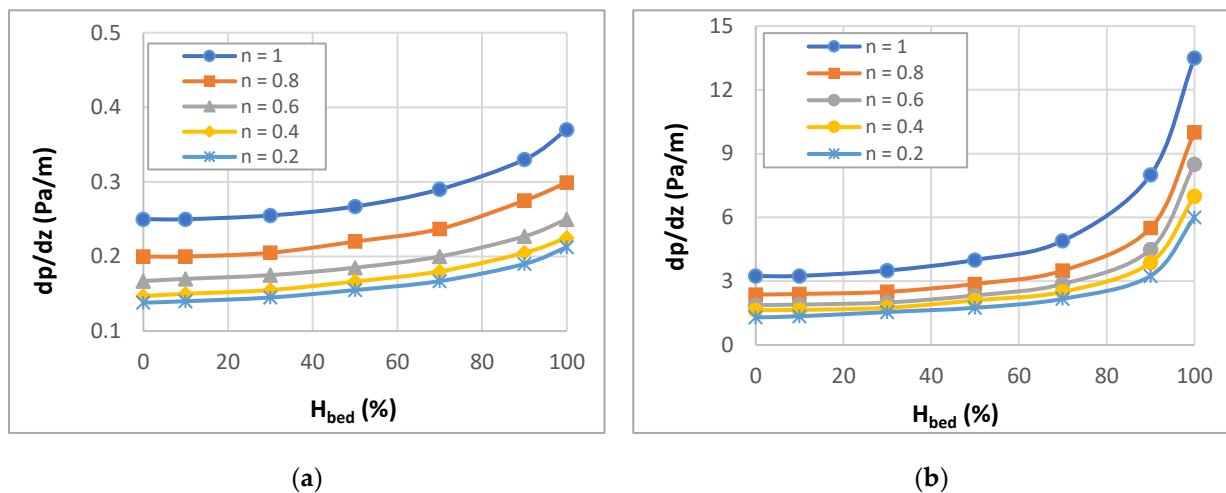


Figure 5. Pressure loss vs. bed height for conditions $e = 0.9$ and $Q = 5 \times 10^{-5} \text{ m}^3/\text{s}$ and different diameter ratios: (a) $k = 0.25$; and (b) $k = 0.75$.

5.2. Shear Stress Distribution

5.2.1. Overall Wall Shear Stress

The average/overall wall shear stress ($\bar{\tau}_w$) is a hydraulic parameter used to evaluate hole cleaning performance. In Figure 6, the overall wall shear stress ($\bar{\tau}_w$) is presented versus dimensionless bed height for various values of fluid behavior index. The wall shear stress in the wellbore increased with bed height. This is anticipated since the wall shear stress and the pressure loss are directly related according to Equation (4). At a constant flow rate, the mean fluid velocity increases with blockage height resulting in a rise in the wall shear stress. Moreover, the wall shear stress is significantly influenced by the fluid behavior index. It reduces considerably with the improvement of the shear-thinning behavior of the fluid.

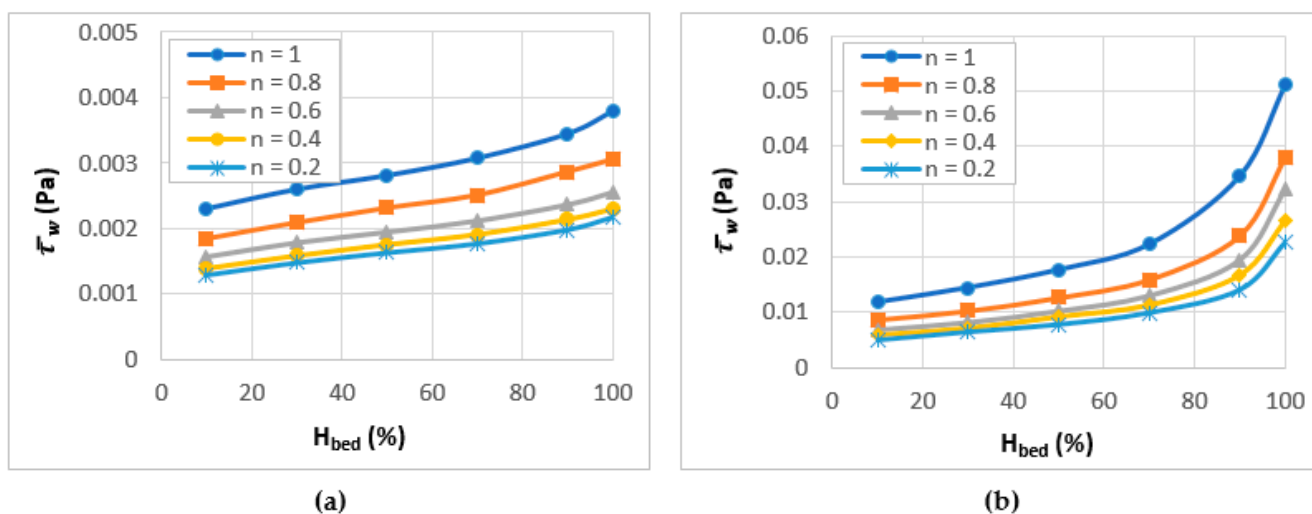


Figure 6. Wall shear stress vs. bed height for conditions $\epsilon = 0.9$ and $Q = 5 \times 10^{-5} \text{ m}^3/\text{s}$ and different diameter ratios: (a) $k = 0.25$; and (b) $k = 0.75$.

5.2.2. Average Bed Shear Stress

Figure 7 displays the average bed shear stress versus the dimensionless bed height for different fluid behavior indexes and diameter ratios. When the flow rate is constant, the bed shear stress increases significantly with the diameter ratio and bed height. This is predominantly due to the reduction in the flow area, which increases the mean fluid velocity. Besides this, the increase in bed shear stress is partly due to the bed approaching the high-velocity core zone of the flow (Figure 8). Consistent with this observation, a recent experimental study [29] demonstrated that the cleaning of eccentric annuli becomes more challenging as the bed gets smaller and the bed shear stress diminishes. Consequently, the Reynolds stresses which help the lifting of bed particles significantly reduces as the bed thickness decreases [30]. The bed shear stress also slightly increases with the fluid behavior index.

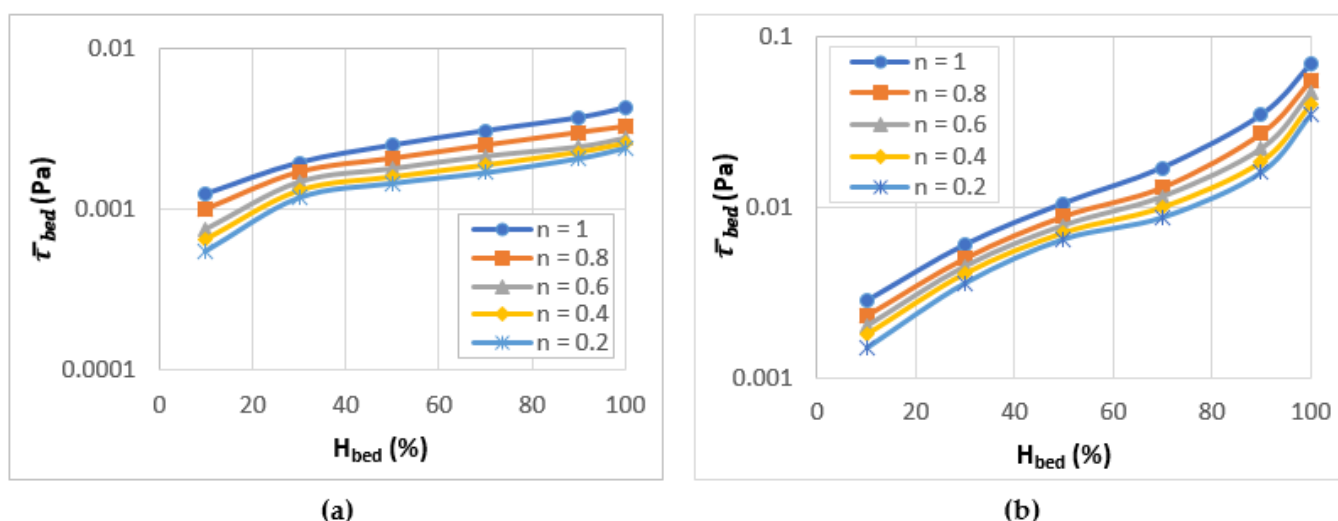


Figure 7. Average bed shear stress vs. bed height for conditions $\epsilon = 0.9$ and $Q = 5 \times 10^{-5} \text{ m}^3/\text{s}$ and different diameter ratios: (a) $k = 0.25$; and (b) $k = 0.75$.

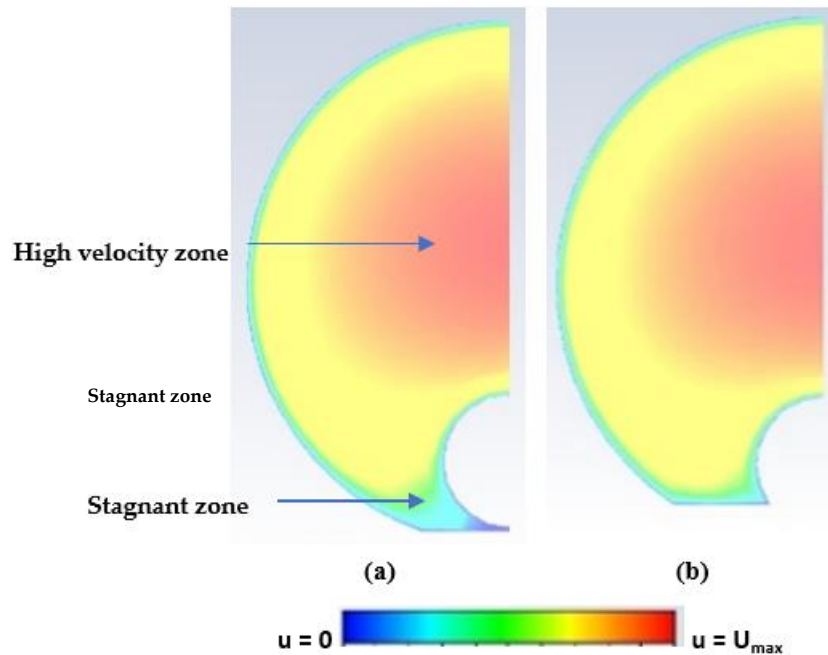


Figure 8. Velocity distributions in partially blocked annuli for case $n = 1, k = 0.25, e = 0.9, Q = 5 \times 10^{-5} \text{ m}^3/\text{s}$ and different bed heights: (a) $H_{bed} = 10\%$; and (b) $H_{bed} = 30\%$.

5.2.3. Dimensionless Bed Shear Stress

Figure 9 presents the dimensionless bed shear stress as a function of dimensionless bed height (H_{bed}), fluid behavior index, and diameter ratio. The bed shear stress increases with bed height and approaches the overall bed shear stress when the H_{bed} reaches 100% (i.e., fully buried inner pipe case). This demonstrates the weakening of the flow stagnation effect which causes the bed shear stress to diminish once the bed surface is below the inner pipe. In addition, all the bed shear stress curves converge as the H_{bed} approaches 100%, showing the reduction in the influence of fluid behavior index on dimensionless bed shear stress.

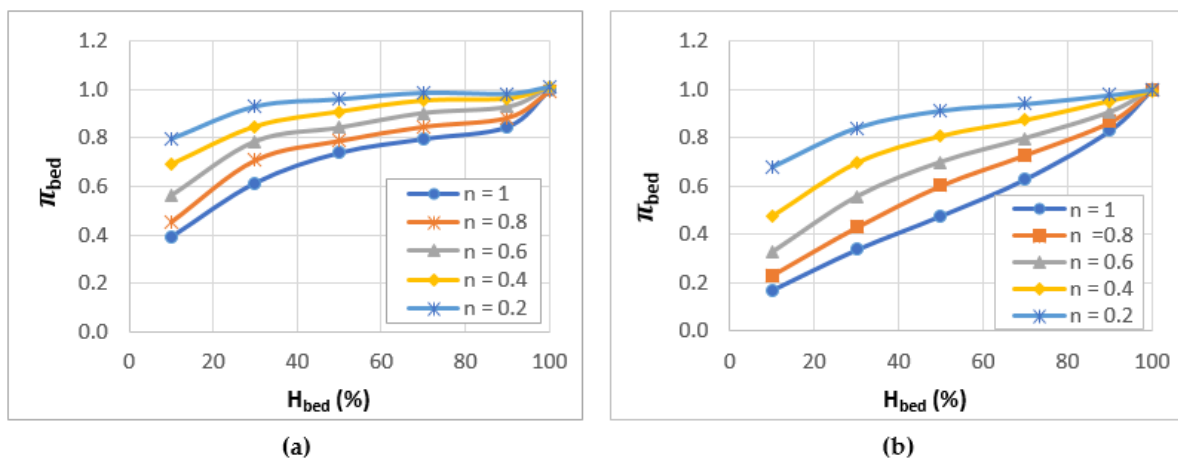


Figure 9. Dimensionless bed shear stress vs. bed height for conditions $e = 0.9$ and $Q = 5 \times 10^{-5} \text{ m}^3/\text{s}$ and different diameter ratios: (a) $k = 0.25$; and (b) $k = 0.75$.

6. Modeling Bed Shear Stress

Average bed shear stress prediction is essential to optimize hole cleaning process and manage wellbore pressure. The dimensionless bed shear stress (π_{bed}) is useful to predict the bed shear stress from the overall wall shear stress, which is calculated from the pressure gradient as shown in Equation (4). The impacts of flow and fluid parameters on the dimensionless bed shear stress are shown in Figure 9. Other fluid and flow parameters that are not shown in the figure such as fluid consistency index, flow rate, Reynolds number can be relevant; and therefore, their impacts on π_{bed} are investigated. These parameters are varied to perform a sensitivity analysis under turbulent flow conditions. The effect of flow rate, Reynolds number, and fluid consistency index on the dimensionless bed shear stress is minor. Applying a non-linear regression analysis, a correlation is developed for the dimensionless bed shear stress. The correlation relates the bed shear stress to the bed height, diameter ratio, and flow behavior index. The simulation data generated during this investigation is used in the development of the correlation. Thus, the dimensionless bed shear stress is expressed as:

$$\pi_{bed} = \hat{A}H_{bed}^{4.5} + \hat{B}H_{bed}^{2.5} + \hat{C}H_{bed}^{0.51} + \hat{D}n\kappa^{0.51} + \hat{E}(nH_{bed})^{1.4} + \hat{F}n + \hat{G} \quad (13)$$

where the coefficients \hat{A} , \hat{B} , \hat{C} , \hat{D} , \hat{E} , \hat{F} and \hat{G} have the following values: $\hat{A} = 0.492985$, $\hat{B} = -0.790858$, $\hat{C} = 0.859049$, $\hat{D} = -0.5004261$, $\hat{E} = 0.487752$, $\hat{F} = -0.285120$, $\hat{G} = 0.555855$. The correlation is applicable for turbulent flow of power-law fluid in eccentric ($90\% \pm 10\%$) annuli with a uniform blockage and diameter ratio ranging from 0.25 to 0.75. Also, it is applicable for fluids with a power-law index ranging from 0.2 to 1.0. Besides this, the dimensionless bed height must be between 0.1 and 1.0 to obtain an accurate prediction of the bed shear stress. To validate the correlation, predictions are compared with simulation data (Figure 10). The predictions of the correlation are found to agree with CFD simulations displaying predominantly a disagreement level of less than 10%.

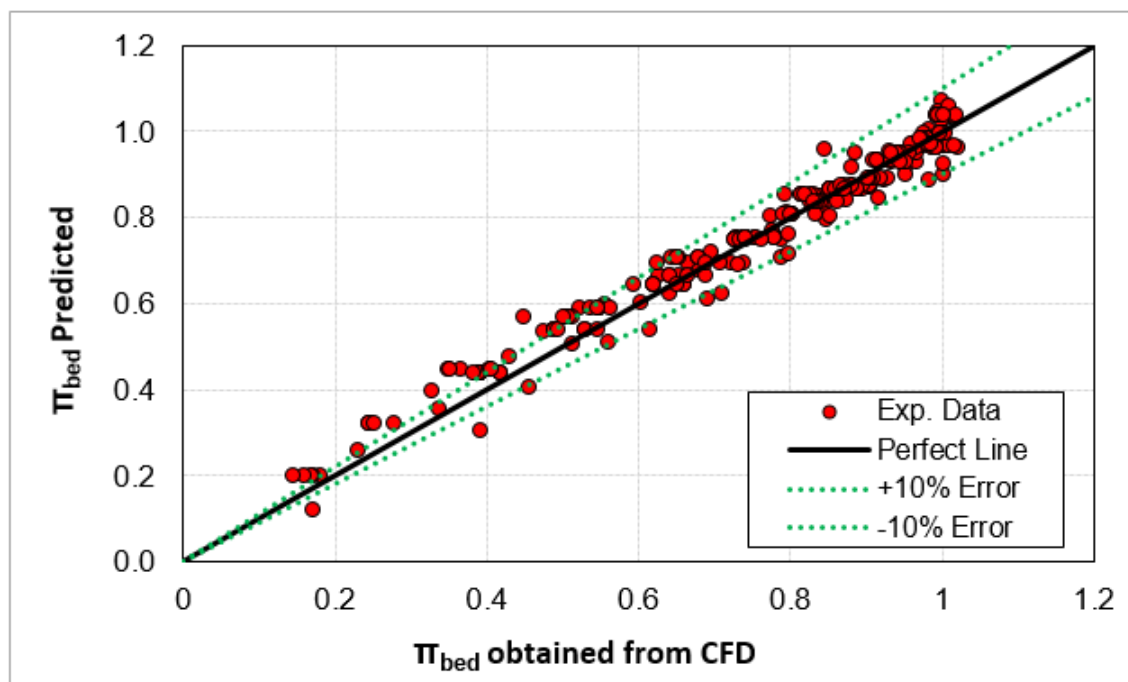


Figure 10. Dimensionless bed shear stress correlation predicted vs. CFD for conditions [$0.25 \leq \kappa \leq 0.75$, $e = 0.9$ and $Q = 5 \times 10^{-5} \text{ m}^3/\text{s}$].

7. Conclusions

A CFD study is conducted under turbulent flow conditions to investigate wellbore hydraulics for a power-law fluid in inclined and horizontal wells. Extensive simulations are conducted varying the cuttings bed height, fluid behavior index, and wellbore diameter ratio. The main contribution of this study is the development of the bed shear stress model by analyzing the simulation results. Besides this, the following conclusions can be made based on the findings of this investigation.

- The dimensionless bed shear stress is a crucial flow parameter in eccentric annuli, which is primarily affected by the bed height, diameter ratio, and fluid behavior index.
- The bed shear stress is a function of dimensionless bed shear stress and overall shear stress, which is affected by mean fluid velocity, wellbore size, diameter ratio, the thickness of the cuttings bed, and properties of the fluid.
- The thickness of the cuttings bed strongly affects the annular pressure gradient. Its impact is more pronounced when the dimensionless bed height is greater than 50%. This is primarily because of the decrease in the flow cross-section area.
- CFD simulation of turbulent flow provides a reasonable prediction of relevant flow parameters including pressure gradient, bed shear stress, and velocity profile.

8. Recommendations for Future Research

The following topics are recommended for future studies in the area of wellbore hydraulics and hole cleaning in inclined wells and better understand non-Newtonian fluid flow in partially blocked eccentric annuli:

- Studying the impact of bed roughness and irregularities on frictional pressure loss and bed shear stress under turbulent flow conditions in partially blocked eccentric annuli.
- Investigating the influence of inner pipe rotation on bed shear stress and frictional pressure gradient in partially blocked eccentric annuli under turbulent flow conditions.
- Developing dimensionless bed shear stress model for fluids exhibiting yield stress such as yield power-law fluids.
- Studying the effect of multiphase flow pattern and the presence of dispersed cuttings on the hydraulics of eccentric annular flow with some level of blockage.

Author Contributions: R.S. performed CFD simulations, conducted data analysis, and prepared the original draft of the article. R.A. developed the research methodology, developed the simulation test matrix, and reviewed and edited the article. H.K. participated in the project management and reviewed the article. M.N. participated in the project management and reviewed the article. I.H. reviewed the article. All authors have read and agreed to the published version of the manuscript.

Funding: The research was funded by The Qatar National Research Fund grant number [NPRP11S-1228-170140].

Acknowledgments: This publication was made possible by an NPRP award [NPRP11S-1228-170140] from the Qatar National Research Fund (a member of The Qatar Foundation). We would like to express our gratitude and appreciation to the University of Oklahoma and Qatar University for supporting the project.

Conflicts of Interest: The authors declare no conflict of interest.

Abbreviations

Symbols

A	Cross-sectional area of the flow
<i>a</i>	geometric parameter
<i>b</i>	geometric parameter

$C_{1\varepsilon}$	constant
$C_{2\varepsilon}$	constant
$C_{3\varepsilon}$	constant
C_μ	constant
D	diameter of pipe, m
D_h	hydraulic diameter
D_i	inner diameter
D_o	outer diameter
d	distance of central axis of inner and outer cylinder
e	relative eccentricity
f	Fanning friction factor
G_k	turbulent kinetic energy due to mean velocity gradient
G_b	turbulent kinetic energy due to buoyancy
H_{bed}	dimensionless bed height
h	bed height
i	inner
\hat{i}	component in the corresponding direction
\hat{j}	component in the corresponding direction
K	consistency index
k	turbulent kinetic energy
L	length
n	power-law index
P	pressure
P_W	wetted perimeter
dP/dL	frictional pressure loss gradient
Q	flow rate
R	radius, m
R_i	radius of inner cylinder
R_o	radius of outer cylinder
Re^*	Reynolds number of annular flows
Re_g	generalized Reynolds number
S_k	user-defined source term
S_ε	user-defined source term
t	time, s
u	local axial velocity (x -axis), m/s
\bar{V}	mean flow velocity
x	x -axis
dx	changes with x -axis
Y_M	fluctuating dilatation
Greek Symbols	
ε	rate of dissipation
$\dot{\gamma}$	shear rate
μ	viscosity of Newtonian fluid
μ_t	turbulent viscosity/eddy viscosity
μ_a	apparent viscosity
$\mu(\dot{\gamma})$	apparent viscosity, Pa.s
κ	diameter ratio, $\kappa = D_i/D_o = R_i/R_o$
ρ	density, kg/m ³
τ	shear stress
$\bar{\tau}_{bed}$	average bed shear stress
$\bar{\tau}_w$	average wall shear stress
σ	turbulent Prandtl number
π_{bed}	dimensionless bed shear stress
Acronyms	
CFD	Computational Fluid Dynamics

References

1. Hanks, R.W. The Axial Laminar Flow of Yield-Pseudoplastic Fluids in a Concentric Annulus. *Ind. Eng. Chem. Process. Des. Dev.* **1979**, *18*, 488–493. [[CrossRef](#)]
2. Filip, P.; David, J. Axial Couette–Poiseuille flow of power-law viscoplastic fluids in concentric annuli. *J. Pet. Sci. Eng.* **2003**, *40*, 111–119. [[CrossRef](#)]
3. Bicalho, I.C.; Dos Santos, D.; Ataíde, C.H.; Duarte, C.R. Fluid-dynamic behavior of flow in partially obstructed concentric and eccentric annuli with orbital motion. *J. Pet. Sci. Eng.* **2016**, *137*, 202–213. [[CrossRef](#)]
4. Founargiotakis, K.; Kelessidis, V.C.; Maglione, R. Laminar, transitional and turbulent flow of Herschel-Bulkley fluids in concentric annulus. *Can. J. Chem. Eng.* **2008**, *86*, 676–683. [[CrossRef](#)]
5. Ahmed, R.; Miska, S.; Miska, W. Friction Pressure Loss Determination of Yield Power Law Fluid in Eccentric Annular Laminar Flow. In Proceedings of the Wiertnictwo, Nafta, Gaz, Krakow, Poland, 10–12 June 2006; Volume 23/1, pp. 47–53.
6. Ahmed, R.; Miska, S.Z. *Drilling Hydraulics: Advanced Drilling and Well Technology*; Aadnoy, B., Cooper, I., Miska, S., Mitchell, R.F., Payne, M.L., Eds.; Society of Petroleum Engineering: Richardson, TX, USA, 2009; Chapter 4.1; pp. 191–220.
7. Rojas, S.; Ahmed, R.; Elgaddafi, R.; George, M. Flow of power-law fluid in a partially blocked eccentric annulus. *J. Pet. Sci. Eng.* **2017**, *157*, 617–630. [[CrossRef](#)]
8. Tang, M.; Ahmed, R.; He, S. Modeling of yield-power-law fluid flow in a partially blocked concentric annulus. *J. Nat. Gas Sci. Eng.* **2016**, *35*, 555–566. [[CrossRef](#)]
9. Azouz, I.; Shirazi, S.A.; Pilehvari, A.; Azar, J.J. Numerical Simulation of Laminar Flow of Yield-Power-Law Fluids in Conduits of Arbitrary Cross-Section. *J. Fluids Eng.* **1993**, *115*, 710–716. [[CrossRef](#)]
10. Hussain, Q.E.; Sharif, M. Viscoplastic fluid flow in irregular eccentric annuli due to axial motion of the inner pipe. *Can. J. Chem. Eng.* **1997**, *75*, 1038–1045. [[CrossRef](#)]
11. Aworunse, O.A. Modeling of Power-Law Fluid Flow in Annulus with Cutting Bed Buildup. Master’s Thesis, University of Oklahoma, Norman, OK, USA, 2012.
12. Bicalho, I.C.; Mognon, J.L.; Ataíde, C.H.; Duarte, C.R. Fluid dynamics study of the flow and pressure drop analysis of a non-Newtonian fluid through annular ducts with unusual cross-sections. *Can. J. Chem. Eng.* **2016**, *94*, 391–401. [[CrossRef](#)]
13. Escudier, M.; Gouldson, I.; Oliveira, P.J.; Pinho, F.T. Effects of inner cylinder rotation on laminar flow of a Newtonian fluid through an eccentric annulus. *Int. J. Heat Fluid Flow* **2000**, *21*, 92–103. [[CrossRef](#)]
14. Fang, P.; Manglik, R.; Jog, M. Characteristics of laminar viscous shear-thinning fluid flows in eccentric annular channels. *J. Non Newtonian Fluid Mech.* **1999**, *84*, 1–17. [[CrossRef](#)]
15. Sorgun, M. Computational Fluid Dynamics Modeling of Pipe Eccentricity Effect on Flow Characteristics of Newtonian and Non-Newtonian Fluids. *Energy Sources Part A Recover. Util. Environ. Eff.* **2011**, *33*, 1196–1208. [[CrossRef](#)]
16. Sorgun, M.; Ulker, E.; Uysal, S.; Övgü, K. A Numerical Approach for Modeling of Turbulent Newtonian Fluid Flow in Eccentric Annulus. *Tek. Dergi* **2018**, *29*, 8497–8513. [[CrossRef](#)]
17. Singh, A.P.; Samuel, R. Effect of Eccentricity and Rotation on Annular Frictional Pressure Losses with Standoff Devices. In *SPE Annual Technical Conference and Exhibition*; Society of Petroleum Engineers (SPE): Richardson, TX, USA, 2009.
18. Kozicki, W.; Chou, C.; Tiu, C. Non-Newtonian flow in ducts of arbitrary cross-sectional shape. *Chem. Eng. Sci.* **1966**, *21*, 665–679. [[CrossRef](#)]
19. Ramadan, A.; Skalle, P.; Johansen, S. A mechanistic model to determine the critical flow velocity required to initiate the movement of spherical bed particles in inclined channels. *Chem. Eng. Sci.* **2003**, *58*, 2153–2163. [[CrossRef](#)]
20. George, M.; Elgaddafi, R.; Ahmed, R.; Growcock, F. Performance of fiber-containing synthetic-based sweep fluids. *J. Pet. Sci. Eng.* **2014**, *119*, 185–195. [[CrossRef](#)]
21. Rojas, S. Flow of Power-Law Fluid in a Partially Blocked Eccentric Annulus. Master’s Thesis, University of Oklahoma, Norman, OK, USA, 2016.
22. Azouz, I.; Shirazi, S.A. Evaluation of Several Turbulence Models for Turbulent Flow in Concentric and Eccentric Annuli. *J. Energy Resour. Technol.* **1998**, *120*, 268–275. [[CrossRef](#)]
23. Wilcox, D.C. *Turbulence Modeling for CFD*, 2nd ed.; DCW Industries: Anaheim, CA, USA, 1998; p. 174.
24. Celik, I.B. *Introductory Turbulence Modeling Mechanical & Aerospace Engineering Dept*; West Virginia University: Morgantown, WV, USA, 1999.
25. Singh, R.A. CFD Analysis of Power-Law Fluid in a Partially Blocked Eccentric Annulus under Turbulent Flow Conditions. Master’s Thesis, University of Oklahoma, Norman, OK, USA, 2019. Available online: <https://shareok.org/handle/11244/323246> (accessed on 26 December 2020).
26. ANSYS. *Academic Research Mechanical, Release 18.1, Help System, Coupled Field Analysis Guide*; ANSYS Inc.: Canonsburg, PA, USA, 2019.
27. Adari, R.B. Development of Correlations Relating Bed Erosion to Flowing Time for Near Horizontal Wells. Master’s Thesis, University of Tulsa, Tulsa, OK, USA, 1999.
28. Adari, R.B.; Miska, S.; Kuru, E.; Bern, P.; Saasen, A. Selecting Drilling Fluid Properties and Flow Rates For Effective Hole Cleaning in High-Angle and Horizontal Wells. In *SPE Annual Technical Conference and Exhibition*; Society of Petroleum Engineers (SPE): Richardson, TX, USA, 2000.

-
29. Bizhani, M.; Kuru, E. How Does a Stationary Sand Bed Affect the Flow Dynamics in an Eccentric Annulus? In Proceedings of the American Society of Mechanical Engineers, Glasgow, UK, 9–14 June 2019.
 30. Bizhani, M.; Kuru, E. Turbulent Flow of Polymer Fluids Over the Sand Bed in Horizontal Concentric Annulus. *Flow Turbul. Combust.* **2018**, *102*, 589–612. [[CrossRef](#)]